4D imaging of cardiac trabeculae contracting in vitro using gated OCT

Ming L. Cheuk, *Student Member, IEEE*, Alexander J. Anderson, *Student Member, IEEE*, June-Chiew Han, Norman Lippok, Frédérique Vanholsbeeck, Bryan P. Ruddy, *Member, IEEE*, Denis S. Loiselle, Poul M.F. Nielsen, *Member, IEEE,* and Andrew J. Taberner, *Member, IEEE*

***Abstract*— Cardiac trabeculae are widely used as experimental muscle preparations for studying heart muscle. However, their geometry (diameter, length, and shape) can vary not only amongst samples, but also within a sample, leading to inaccuracies in estimating their stress production, volumetric energy output, and/or oxygen consumption. Hence, it is desirable to have a system that can accurately image each trabecula in vitro during an experiment. To this end, we constructed an optical coherence tomography (OCT) system and implemented a gated imaging procedure to image actively contracting trabeculae and reconstruct their time-varying geometry. By imaging a single cross section while monitoring the developed force, we found that gated stimulation of the muscle was sufficiently repeatable to allow us to reconstruct multiple contractions to form a 4D representation of a single muscle contraction cycle. The complete muscle was imaged at various lengths and the cross-sectional area along the muscle was quantified during the contraction cycle. The variation of cross-sectional area along the length during a contraction tended to increase as the muscle was contracting, and this increase was greater at longer muscle lengths. To our knowledge, this is the first system that is able to measure the geometric change of cardiac trabeculae in vitro during a contraction, allowing cross-sectional stress and other volume dependent parameters to be estimated with greater accuracy.**

***Index Terms*— biomedical imaging, electromechanical sensors, microscopy, isolated cardiac muscle, optical imaging, optical coherence tomography.**

This paper was submitted for review on 22/03/2016. This work was supported in part by the Marsden Fund Council, administered by the Royal Society of New Zealand (#UOA1108), and the Heart Foundation of New Zealand (#1601, #1611).

M. L. Cheuk (Tel: +64220314159 Email: ming.cheuk@auckland.ac.nz), J.-C. Han and A. J. Anderson are with the Auckland Bioengineering Institute, University of Auckland, New Zealand.

N. Lippok is with the Harvard Medical School and Wellman Center for Photomedicine, Massachusetts General Hospital, Boston, Massachusetts 02114.

F. Vanholsbeeck is with The Department of Physics, University of Auckland, New Zealand.

D. S. Loiselle is with the Department of Physiology and Auckland Bioengineering Institute, University of Auckland, New Zealand.

B. P. Ruddy, P. M. F. Nielsen, and A. J. Taberner are with the Auckland Bioengineering Institute and the Department of Engineering Science, University of Auckland, New Zealand.

I. Introduction

Heart disease is a significant cause of death worldwide. Because of this, the study of the mechanics of myocardial tissue is a major international undertaking. A serious limitation to this undertaking is the complicated arrangement of muscle cells within the 3D geometry of the heart [1]. This limitation can be mitigated through the experimental use of trabeculae that can be found on the endocardial surfaces of the chambers. Trabeculae are the smallest naturally-arising collections of linearly arranged cardiac myocytes present in the heart [2]. Their simple architecture makes them useful for the study of cardiac muscle mechanics.

Controlled experiments on isolated trabeculae are performed in order to better understand the biomechanical processes and changes that occur in the heart during each beat. Typically, samples are placed in an oxygenated experimental solution to maintain their viability, and are stimulated chemically or electrically to contract. Several parameters such as force, sarcomere length, intracellular calcium concentration, and energy can be measured [3]–[5]. These measurements are combined to build a better picture of the key processes that occur in both healthy and diseased muscle.

However, a problem common to all studies of isolated muscles arises when quantifying their stress (force per cross-sectional area) development: cross-sectional area generally varies along the length of the muscle. Until recently, the common practice has been to estimate a single diameter of the preparation at mid-length and calculate cross-sectional area based on the assumption of circularity [5]–[7]. Some [8] have improved upon this ‘single-view’ method by measuring ‘width’, from the top view, prior to rotating the trabecula 90° around its long axis in order to estimate ‘thickness’. More recently, using a simple mirror arrangement, two orthogonal diameters have been measured and an elliptical cross section assumed [9], [10]. However, these approaches can lead to errors when the muscle cross section cannot be adequately modeled by a circle or ellipse, and/or is not uniform along muscle length. More importantly, this approach does not provide information about the local stress that any cross section experiences at any time. Therefore, it is crucial to measure the full 3D geometry of the muscle to quantify accurately muscle stress and volumetric energy output.

Optical Coherence Tomography (OCT) is an imaging

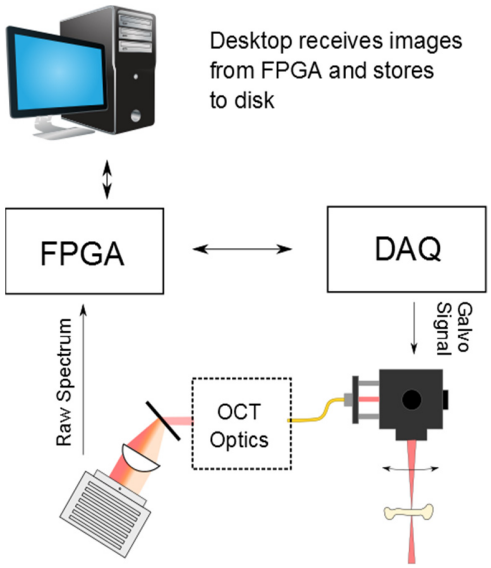

Fig. 1. System diagram of the gated OCT system.

technique based on low coherence interferometry that provides three-dimensional images of tissue reflectance [11]. OCT has been used to image the structures of the retina, gastrointestinal tissue, arteries, and embryonic hearts [12]–[14]. The principles of this imaging technique can also be applied to the estimation the elastic properties of soft tissues [15]. We have previously demonstrated the use of OCT in imaging chemically-fixed trabecula samples mounted in a fluid bath, at a resolution of 3.6 µm × 23 µm × 23 µm (D × L × W) [16].

In this study, we added OCT to our motorized muscle experimentation rig, enabling, for the first time, 3D imaging of contracting trabeculae and the measurement of changes in geometry during contraction. Previous methods to image isolated trabeculae in 3D have required the muscle to be chemically fixed and imaged in a separate device, with no possibility of imaging during normal contraction [17]. In this paper, we describe the implementation of OCT imaging in a muscle rig. We present results from imaging an actively contracting trabecula from an adult rat heart, and discuss the new types of isolated muscle studies that this system enables.

II. Methods

A. Optical Coherence Tomography

A spectral domain OCT was built in-house to perform a volumetric scan of a cardiac trabecula [16], [18]. A superluminescent diode with a center wavelength of 840 nm and a spectral width of 90 nm (Broadlighter D-840, Superlum) provided the light source. A 2D galvanometer steered the laser through the specimen (GVSM002/M, Thorlabs). The reflected light was collected and combined with the reference signal. Using a transmission volume phase holographic grating, the interference spectrum was imaged on a 2048 pixel line scan camera (spL2048-70km, Basler). A schematic of the system is shown in Fig. 1.

The galvanometer was controlled by a data acquisition card (DAQ) using a 16-bit analog signal (NI 6259, National Instruments). The spectrometer camera was synchronized over a hardware connection with the sample clock of the DAQ to ensure that every acquisition was synchronized with the galvanometer movement. To assist with gated acquisition, the stimulus signal was directly read by the DAQ, which synchronized the galvanometer movement to the stimulus signal.

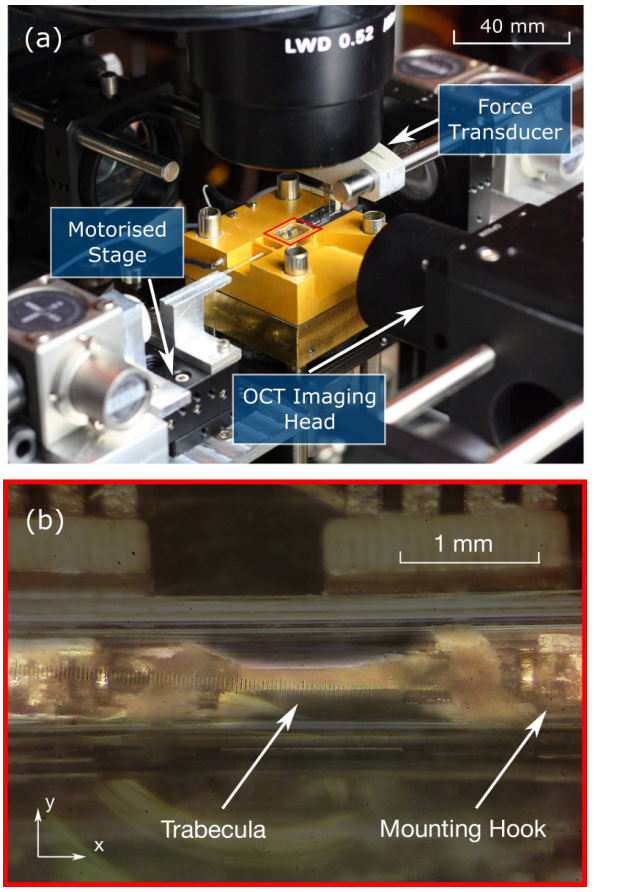

Fig. 2. (a) An overview of the imaging system. There are two voice coil motors (one on each side of the bath) that are each fixed to a platinum hook. A force transducer is attached to one of the hooks. The OCT looks into the bath from the front. The trabecula is mounted at the center of the bath, as outlined in red. A close-up, top-down view of this is shown in (b).

The spectral signal was read by a field programmable gate array (FPGA) over a camera link interface (NI 1483R, National instruments). The FPGA was able to perform 90,000 acquisitions, linearizations, and Fourier transforms per second to transform the signal into a depth intensity map. In practice, the maximum line rate was limited by the 25 µs exposure time needed for acceptable signal-to-noise ratio, corresponding to 40,000 A-scans per second. The processed A-scans were streamed to a desktop computer running Windows and saved directly to two solid-state drives in RAID-0 configuration supporting a maximum sequential throughput of 942 MB/s.

Depth resolution was calibrated using a reference glass slide, and was found to be 3.17 µm per pixel. The galvanometer displacement was calibrated using a negative 1951 USAF resolution test target [16].

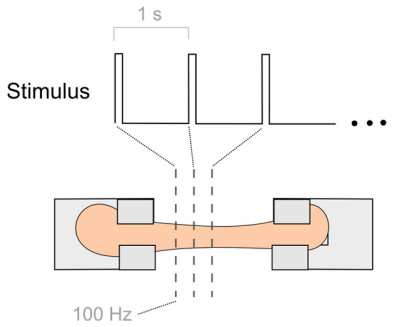

Fig. 3. Illustration of the scanning routine. At each rising edge of the stimulus, the laser is moved to a new plane. Each plane is imaged at a B-Scan rate of 100 Hz during the course of the contraction.

B. Muscle Rig

The OCT was installed in a muscle rig purpose-built for in vitro trabecula studies (Fig. 2). The muscle was attached between two platinum hooks and enclosed by an open-ended square glass capillary tube with an inner width of 1 mm. Oxygenated superfusate flowed through the capillary, delivered using gravity feed. The supporting structure of the bath and incoming fluid path was made of tellurium copper, plated in gold, and coated in Parylene to provide electrical isolation. Platinum electrodes were placed on each side of the bath to provide electric field stimulation.

Each hook was connected to a feedback-controlled voice coil motor for positioning. The position of each hook was measured using a heterodyne laser interferometer, with a resolution of ~0.3 nm [19]. When the interferometer was used to measure the displacement of a steel cantilever, (k = 1400 N/m calibrated using a load-cell (FUTEK LSB200), resonant frequency ~1100 Hz) the noise-equivalent force was 2.23 μN, as quantified by the standard deviation of noise over a measurement bandwidth of 1 kHz.

Located below the muscle bath on an axis orthogonal to the OCT was a 40× microscope objective that imaged an area of 270 μm × 270 μm, imaging sarcomeres to a resolution of 0.264 μm/pixel. The muscle was transilluminated by a condenser, using a halogen white-light source.

C. Sample Preparation

A muscle experiment was conducted in accordance with protocols approved by the Animal Ethics Committee of the University of Auckland.

An unbranched trabecula, with small blocks of ventricular wall at each end, was dissected from the right ventricle of an adult Wistar rat. The sample was mounted in the capillary and superfused with oxygenated Tyrode's solution (130 mmol/L NaCl, 6 mmol/L KCl, 1 mmol/L $MgCl_2$, 0.5 mmol/L NaH_2PO_4, 1.0 mmol/L $CaCl_2$, 10 mmol/L Hepes, 10 mmol/L glucose; pH adjusted to 7.4 using Tris) at room temperature. A 10 V, 10 ms stimulation was applied at a rate of 2 Hz for a period of 20 minutes to allow the muscle to equilibrate with the new environment. After the sample had equilibrated (as assessed by its steady force production), it was stretched in 50 μm steps to optimal length (L_o) – the length that gives the highest active force without significantly increasing the passive tension. The muscle was allowed to settle for 1 min between length steps.

D. Microscope Imaging

The muscle sample was imaged using the microscope to confirm the sarcomere spacing corresponding to optimal length. Sarcomere length was estimated by counting visible sarcomeres and dividing the known distance by the count. The microscope was also used to image the hook region where the muscle was attached, to reveal any in-plane motion in that region during activation and stretching. This region of the muscle is normally obscured from the view of the OCT by the opaque hooks.

E. Stability of Contractions over Imaging Period

For accurate reconstruction of the geometry during a single twitch, it was important that the muscle contractions were repeatable along the length of the muscle during the entire imaging period. This requirement was tested by comparing OCT cross-section images gathered at the same muscle location and phase in the contraction cycle using a similarity metric, the sum of absolute differences (SAD), defined as:

$$SAD = \sum_{(i,j)\in W} |A_1(i,j) - A_2(i,j)| \qquad (1)$$

where A_1 and A_2 represent the cross-sectional images at two different time points and i and j are indices of the pixels.

The first step was to establish a measure of baseline repeatability between images gathered under identical conditions. The center cross section of a quiescent trabecula was imaged 100 times. The first 50 images were averaged to reduce the effects of inherent time-varying OCT noise. Similarly, the last 50 images were averaged together. The SAD was computed between the two averaged images to provide a baseline score.

Next, the same trabecula was stimulated at a rate of 2 Hz and imaged during a total of 500 contractions (a figure which exceeds the 200 scans required to image an entire muscle). A total of 50 images during systole (peak force development) at the beginning of the imaging period were selected and averaged, and compared to the average of another 50 images of the same systolic cross-section gathered at the end of the sequence. The SAD between the two averaged sets quantified the similarity between contractions at the beginning and end of the imaging cycle. Additionally, 50 images averaged in diastole were compared to 50 images averaged in systole, to quantify the SAD between two completely different points in contraction.

Force data for this period were also recorded. The change in systolic force during the imaging period was expressed as a percentage of the initial systolic force.

F. Scanning Routine

Imaging an actively contracting trabecula presents an additional challenge over imaging a stationary muscle. The

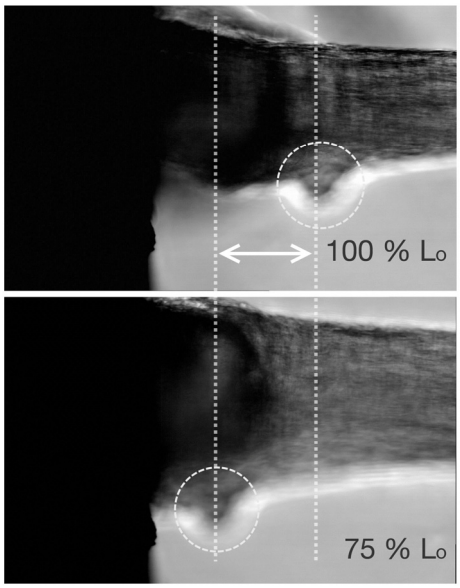

Fig. 4. The microscope images of the mounting points at two different states of stretch. The movement of the circled feature highlights the displacement of tissue with respect to the hook when shortened from 100 % L_O to 75 % L_O. As a result, the OCT is expected to image a larger volume at 100 % L_O.

OCT system captures volumetric data in a raster scan pattern. The time to acquire geometric data from a volume of 2000 µm × 500 µm × 500 µm is 1 s, which is far too protracted to resolve the changes in geometry during a single contraction (~300 ms). To circumvent this constraint, the imaging process was spread over several contractions. During each contraction cycle, only one 2D cross section was imaged, at a rate of 100 Hz.

It is important that the scans between contractions are in phase with one another, so they can be reconstructed as a single contraction. To this end, the acquisition was gated to the stimulus signal. This is an approach previously taken by Jenkins et al, who performed gated OCT imaging on rat and avian embryonic hearts by either gating to the field stimulator, or to the blood flow measured by a Doppler shift [14], [20]. By gating the signal to the field stimulator, the acquisition cycle was always in phase with the contraction cycle.

In all scans, the 2D galvanometer was set to increment at 10 µm per step in both axes, and the A-scan rate was set to 20 kHz. Prior to the experiment, 1000 background spectra were averaged, stored, and subsequently subtracted from all of the following spectra obtained from the sample. This step reduced the coherence noise in the image [21].

1) Active Contraction at Single Length

The start of each acquisition sequence was triggered by the rising edge of the stimulus signal, as depicted in Fig. 3. This ensured that time points were in phase between cross sections. After the same cross section was imaged 100 times during the course of a single twitch, the galvanometer was moved to the next cross section. This process was repeated along the length of the muscle. The entire muscle was imaged twice in order to compare and average.

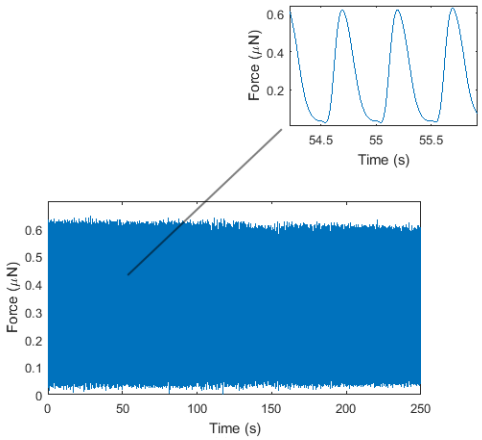

Fig. 5. Force trace of the signal over 500 contractions. It shows that the force amplitude is reasonably constant over the period of imaging.

The time it took to image a complete muscle using this method depended on the length of the specimen and stimulation rate. Thus, when a 2.0 mm muscle was stimulated at a rate of 1 Hz, a single scan of its entire volume took 200 s to complete.

The recorded data included a time stamp and the position along the muscle for every frame. This enabled the reconstruction of 3D data independent of the order in which the images were acquired. The cross sections along the length of the muscle were imaged in random order. By randomizing the scan, any sequential motion along the muscle in the reconstructed model was unlikely to appear as an artifact of the scanning pattern.

2) Varying Muscle Length

The above sequence was then repeated while the muscle was held at different lengths to determine changes in the distribution of cross-sectional area with length. From optimal length (L_o), the muscle was shortened to 95 %, 90 %, 85 %, 80 %, and 75 % of L_o sequentially. At each length, the entire muscle was imaged with the OCT system once the force trace had stabilized, while it was stimulated at 2 Hz.

G. Image Processing

The regions containing the mounting hooks were excluded by manual identification of the tips of the hooks in the OCT images and excluding all slices outside of these bounds.

A 3D Gaussian filter with a standard deviation of 2 pixels was applied to the OCT images to reduce the high frequency speckle noise in the images [22]. Prior to segmentation, the images were re-sampled at 3× resolution using tricubic interpolation. This step smoothed the edges of the binary image in all axes.

Finally, the images were segmented using binary thresholding in the image processing tool *Fiji* [23]. The threshold was automatically selected iteratively using a method described by Ridler et al. in 1978 [24].

H. Analysis

The cross-sectional area of the muscle was computed for

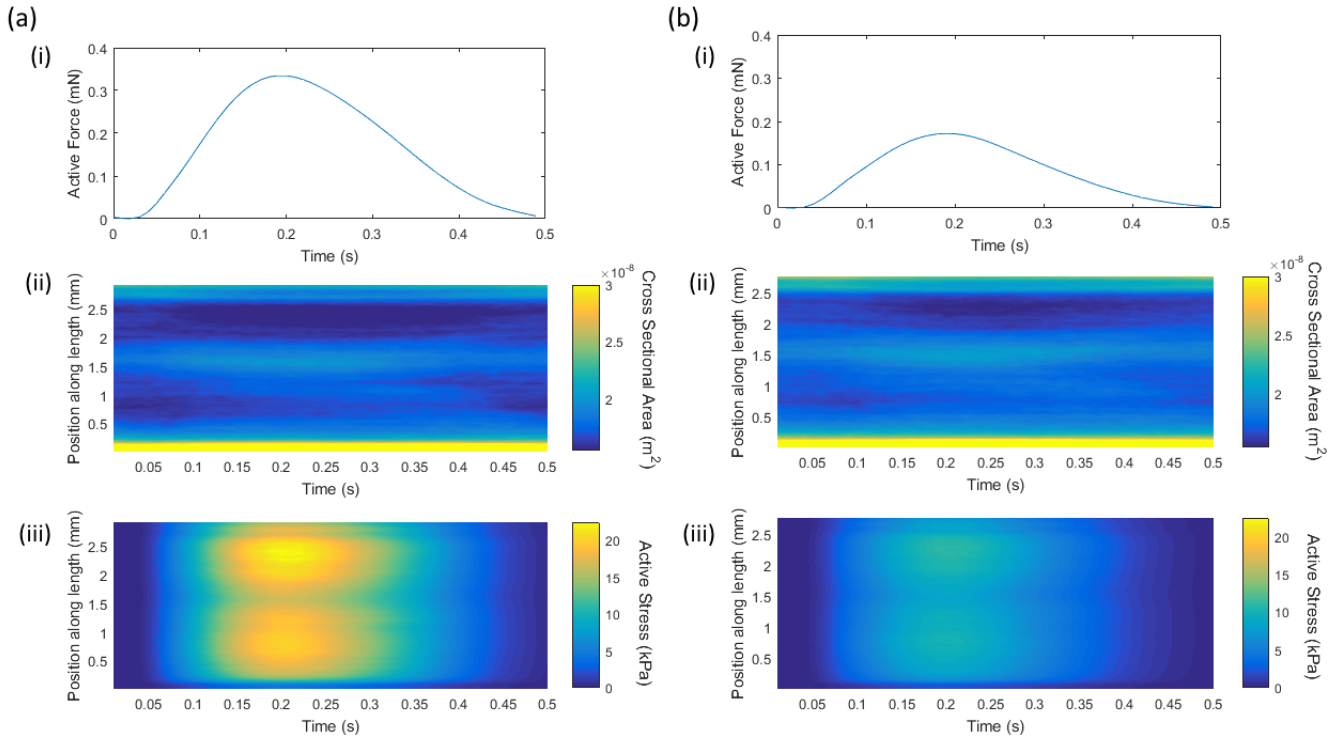

Fig. 6. Simultaneous measurements of active force and cross-sectional area at (a) optimal length (L_O) and (b) 95 % L_O . (i) plots the average force measured by the transducer. (ii) shows the cross-sectional area (color axis) along the length of the muscle (y-axis) throughout the contraction cycle (x-axis). Similarly, (iii) shows the average stress (color axis) over the length of the muscle (vertical axis) plotted over time (horizontal axis).

each segmented slice by integrating the pixels enclosed by the binary image boundary. Force was assumed to be uniaxial and balanced along the length of the muscle. The average stress at each cross section was found by dividing force measured from the transducer by the cross-sectional area. The muscle volume was calculated by summing the voxels and multiplying by the voxel volume.

The variability of cross-sectional area along the muscle was calculated as an index of non-uniformity. The median absolute deviation (MAD) was chosen as a measure of variability, given its resilience to outlier values such as those that can arise near the ends of the muscle. This estimate was normalized to the average cross-sectional area and expressed as a percentage.

III. Results

A. Microscope Observations

The microscope images revealed the sarcomere spacing, which was verified to be 2.2 µm at optimal length.

When the muscle was lengthened by moving the hooks apart, some of the muscle tissue initially obscured by the hooks was pulled into the field of view of the OCT system (Fig. 4). The displacement of this tissue was estimated to be approximately 102 µm based on manually tracking the feature shown in the figure. This suggests that the total volume of the muscle visible to the OCT would increase with muscle length. During isometric contraction, this motion was much less significant: ~7 µm at 75 % L_O and ~17 µm at optimal length (100 % L_O). This motion was observed to be repeatable across multiple contraction cycles.

B. Stability of Contractions

During the 500 contractions (a duration of > 4 minutes), shown in Fig. 5, the active force development was consistent to within 0.10 %.

The average sum of absolute differences (SAD) between two images of the center of the quiescent muscle was 51,992. The SAD between two images at peak contraction was 58,073. The SAD between images during rest and at peak force (where area change is the greatest) was 105,090. This showed that the differences between images were mostly due to frame to frame noise, rather than inconsistent muscle contraction or out of phase imaging.

C. Active Contraction (Single Length)

Fig. 6 (a)(i) and 6 (b)(i) show the average force over a contraction period as measured by the force transducer. The peak force occurs 0.20 ms after the onset of stimulation.

The geometric data reveal the change in cross-sectional area along the muscle. Fig. 6 (a)(ii) shows the cross-sectional area at each position along the length of the muscle, plotted over time. It appears that there is a change in cross-sectional area at various sections over the course of a contraction.

Combining the force data with the geometry, we can determine the local stress as a function of time, as shown in

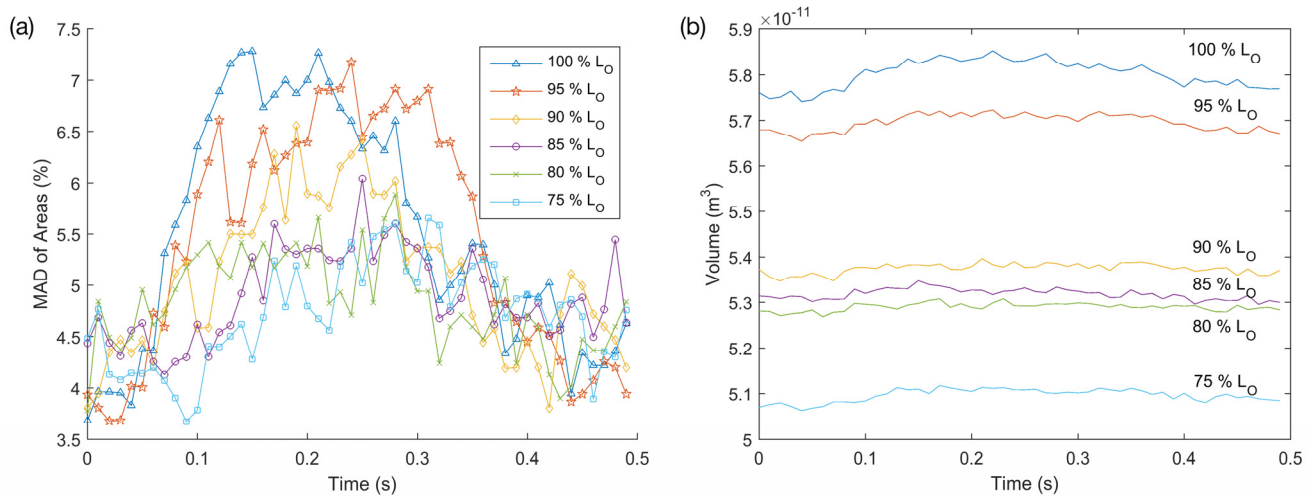

Fig. 7. (a) The median absolute deviation (variation) in cross-sectional area along the length of the muscle as a function of time, plotted for each muscle length. (b) The volume of the muscle during the course of contraction at different muscle lengths.

Fig. 6 (a)(iii). Inevitably, the average stress is greatest at the regions of the muscle where cross-sectional area is low (2.0 mm to 2.5 mm and 0.5 mm to 1.4 mm). The variation in average cross-sectional stress along the length of muscle, as calculated from the MAD, was 7.25 % at peak force.

D. Changing Muscle Length

The uniformity in cross-sectional area as the muscle was contracting is shown in Fig. 7 (a), where a higher MAD implies greater non-uniformity. It appeared that the muscle was least uniform during diastole at all lengths. However, the decrease in uniformity was greatest when the muscle was stretched to optimal length.

Fig. 7 (b) displays the volume of the muscle at different muscle lengths. The observed volume increased as the muscle was stretched, as predicted by the microscope images at the ends of the muscle. It appeared that the greatest change in observed volume during a contraction (~3 %) occurred when the muscle was stretched to optimal length.

IV. Discussion

A. Decreasing Imaging Time

The time required for a single scan is inherently set by the stimulation frequency. The OCT scans one cross section until the entire contraction is complete, even though the A-scan rate could be higher. The OCT scan rate could be increased by scanning lengthwise across the muscle instead of transversely. This would reduce the imaging time 5-fold to 30-fold, depending on the aspect ratio of the muscle, reducing the chance of muscle properties changing during the imaging process. However, the disadvantage is that muscles can be longer than 2.5 mm, requiring at least 250 A-scan steps. The time interval between each data point in each frame would be between 5-fold and 30-fold greater, reducing the ability to capture rapid motion across the muscle without blurring.

There is further potential to increase the scanning rate by using a Fourier domain mode locked laser. The fastest FDML currently has an A-Scan rate of about 5 MHz at 1300 nm [25]. In theory, this source could enable the entire volume of the muscle to be imaged at a rate of 84 Hz. This setup would also need a resonant scanner capable of at least 16 kHz to support that scanning speed.

B. Stress distribution

The variation in cross-sectional area along the muscle can result in equally large variation in cross-sectional stress. This shows the significance that the geometry has in analyzing the mechanics of the sample, and the advantage an accurate geometric model has over a simple cylindrical model. Additionally, an interesting phenomenon is revealed in Fig. 6(b), where two regions (0.5 mm - 1 mm and 2 mm - 2.5 mm) started with approximately the same cross-sectional areas but behaved differently at peak of contraction, when one increased and the other decreased in area. This phenomenon could reflect a different proportion of active sarcomeres in the two regions. An interesting follow-up study would be to analyze the local sarcomere length to see whether the difference in change of cross-sectional area is reflected in the sarcomere shortening/lengthening.

During a contraction, the deformations are tracked, which can also be built into the model. The results in Section III. D. show that changing the pre-strain also had an effect on the distribution of cross-sectional areas, and hence stress. This could have interesting effects on work-loop experiments where the muscle is changing in length during contractions.

The stresses calculated in this study are indicative of the average stress across a B-scan. A more detailed stress analysis could be performed by creating a geometric model with passive mechanical properties obtained from experimental data. Boundary conditions that match the attachment mechanism could be applied to the ends of the simulated muscle, and the stress distribution could be obtained using finite element methods. This would produce a true 3D passive stress distribution and make use of the detailed geometric data.

C. Changes in volume

The apparent changes in muscle volume were explained by

the movement of tissue in and out of the field of view of the OCT, from the results of microscopic imaging in Section III. This effect was most significant when the muscle was lengthened or shortened. Tissue movement at the hook ends was also present during isometric contractions, although to a lesser degree, and is evident in the volume plots (Fig. 7 (b)). This suggests that studies that seek to relate changes in volume to physiological changes will require modifications to the setup, either by using transparent hooks or other no-slip attachment mechanisms. Alternatively, specific sections of muscle that always lie within the field of view of the OCT could be tracked, possibly with the use of additional markers.

D. In-plane motion

In-plane motion normal to the OCT slices is currently not accounted for, and it is shown in the transmission images that there is indeed in plane movement, especially at the ends of the muscle. Consequently, the changes in cross-sectional area at various location of the muscle may not reflect the same cross section.

One way to measure this is to track internal features in the OCT using motion estimation techniques. However, this is difficult to achieve with OCT alone as the resolution is too low to capture internal structure. It is possible to see in-plane motion for some preparations with features on the surface of the muscle, but this is not consistent across experiments.

In future experiments we plan to combine the surface geometry acquired from OCT with feature tracking using another technique, such as markers and transmission imaging. This will then enable us to track cross-sectional changes for specific sections of the muscle.

V. CONCLUSIONS

We have demonstrated geometric measurement of actively contracting muscle using OCT. The image data over multiple contractions have been reconstructed into a single representative 3D contracting model, and the validity of this type of reconstruction has been confirmed through repeated imaging. Combining the geometry with force data, the cross-sectional area and average stress along the length of the muscle were calculated while the muscle was contracting at different preloads.

The 3D geometric information provided by the OCT enables detailed mechanical analyses to be performed using finite element methods. Future work includes adding intracellular Ca2+ and localized sarcomere length measurements to provide more information about the individual contractile units. Combining this information with the model will allow us to study in detail the mechanical effects of localized deactivation of sarcomeres.

REFERENCES

[1] I. J. LeGrice et al., “Laminar structure of the heart: ventricular myocyte arrangement and connective tissue architecture in the dog,” *Am. J. Physiol.*, vol. 269, pp. 571–582, 1995.

[2] J.-C. Han et al., “Interventricular comparison of the energetics of contraction of trabeculae carneae isolated from the rat heart.,” *J. Physiol.*, vol. 591, no. Pt 3, pp. 701–17, 2013.

[3] B. D. Stuyvers et al., “Effect of stimulation rate, sarcomere length and Ca2+ on force generation by mouse cardiac muscle,” *J. Physiol.*, vol. 544, no. 3, pp. 817–830, Sep. 2002.

[4] D. P. Dobesh et al., “Cooperative activation in cardiac muscle: impact of sarcomere length.,” *Am. J. Physiol. Heart Circ. Physiol.*, vol. 282, no. 3, pp. H1055–62, Mar. 2002.

[5] J.-C. Han et al., “A unique micromechanocalorimeter for simultaneous measurement of heat rate and force production of cardiac trabeculae carneae.,” *J. Appl. Physiol.*, vol. 107, no. 3, pp. 946–51, Sep. 2009.

[6] C. Mansfield et al., “Stretch of contracting cardiac muscle abruptly decreases the rate of phosphate release at high and low calcium,” *J. Biol. Chem.*, vol. 287, no. 31, pp. 25696–25705, 2012.

[7] N. Milani-Nejad et al., “Effect of muscle length on cross-bridge kinetics in intact cardiac trabeculae at body temperature.,” *J. Gen. Physiol.*, vol. 141, no. 1, pp. 133–9, 2013.

[8] S. Raman et al., “Effect of muscle dimensions on trabecular contractile performance under physiological conditions,” *Pflugers Arch. Eur. J. Physiol.*, vol. 451, no. 5, pp. 625–630, 2006.

[9] A. J. Taberner et al., “Measuring the mechanical efficiency of a working cardiac muscle sample at body temperature using a flow-through calorimeter,” in *Proceedings of the Annual International Conference of the IEEE Engineering in Medicine and Biology Society, EMBS*, 2015, vol. 2015-Novem, pp. 7966–7969.

[10] C. M. Johnston et al., “A high-resolution thermoelectric module-based calorimeter for measuring the energetics of isolated ventricular trabeculae at body temperature,” *Am. J. Physiol. Hear. Circ. Physiol.*, vol. 309, no. 2, pp. H318–H324, 2015.

[11] Z. Yaqoob et al., “Spectral domain optical coherence tomography: a better OCT imaging strategy,” *Biotechniques*, vol. 39, no. 6 Suppl, pp. S6–13, Dec. 2005.

[12] J. G. Fujimoto, “Optical coherence tomography for ultrahigh resolution in vivo imaging.,” *Nat. Biotechnol.*, vol. 21, no. 11, pp. 1361–7, Nov. 2003.

[13] T. M. Yelbuz et al., “Optical coherence tomography: A new high-resolution imaging technology to study cardiac development in chick embryos,” *Circulation*, vol. 106, no. 22, pp. 2771–2774, 2002.

[14] M. Jenkins et al., “4D embryonic cardiography using gated optical coherence tomography,” *Opt. Express*, vol. 14, no. 2, pp. 736–748, 2006.

[15] B. F. Kennedy et al., “A review of optical coherence elastography: Fundamentals, techniques and prospects,” *IEEE J. Sel. Top. Quantum Electron.*, vol. 20, no. 2, 2014.

[16] M. L. Cheuk et al., “Optical coherence tomography imaging of cardiac trabeculae,” in *Engineering in Medicine and Biology Society (EMBC), 2014 36th Annual International Conference of the IEEE*, 2014, pp. 182–185.

[17] S. Goo et al., “Trabeculae carneae as models of the ventricular walls: implications for the delivery of oxygen.,” *J. Gen. Physiol.*, vol. 134, no. 4, pp. 339–50, Oct. 2009.

[18] N. Lippok et al., “Dispersion compensation in Fourier domain optical coherence tomography using the fractional Fourier transform,” *Opt. Express*, vol. 20, no. 21, pp. 1704–1706, 2012.

[19] A. J. Anderson et al., “An investigation into the viability of image processing for the measurement of sarcomere length in isolated cardiac trabeculae,” in *Engineering in Medicine and Biology Society*

(EMBC), 2012 Annual International Conference of the IEEE, 2012, pp. 1566–1569.

[20] M. W. Jenkins et al., "In vivo gated 4D imaging of the embryonic heart using optical coherence tomography.," *J. Biomed. Opt.*, vol. 12, no. 3, pp. 030505–030505–3, 2007.

[21] M. Wojtkowski, "High-speed optical coherence tomography: basics and applications.," *Appl. Opt.*, vol. 49, no. 16, pp. D30–61, Jun. 2010.

[22] B. Sander et al., "Enhanced optical coherence tomography imaging by multiple scan averaging.," *Br. J. Ophthalmol.*, vol. 89, no. 2, pp. 207–212, 2005.

[23] J. Schindelin et al., "Fiji: an open-source platform for biological-image analysis," *Nat. Methods*, vol. 9, no. 7, pp. 676–682, 2012.

[24] S. Ridler, T.W. Calvard, "Picture Thresholding Using an Iterative Slection Method," *IEEE Trans. Syst. Man Cybern.*, vol. 8, no. 8, pp. 630–632, 1978.

[25] W. Wieser et al., "Multi-megahertz OCT: High quality 3D imaging at 20 million A-scans and 4.5 GVoxels per second.," *Opt. Express*, vol. 18, no. 14, pp. 14685–14704, 2010.